Solid State Communications 174 (2013) 26–29

Contents lists available at ScienceDirect

Solid State Communications

journal homepage: www.elsevier.com/locate/ssc

# Magnetoelastic interactions in Raman spectra of $Ho_{1-x}Nd_xFe_3(BO_3)_4$ crystals

Alexander S. Krylov*, Svetlana N. Sofronova, Irina A. Gudim, Alexander N. Vtyurin

*L.V. Kirensky Institute of Physics SB RAS, 660036 Krasnoyarsk, Russia*

ARTICLE INFO

*Article history:*
Received 3 December 2012
Received in revised form
31 July 2013
Accepted 10 September 2013
by D.D. Sarma
Available online 17 September 2013

*Keywords:*
A. Multiferroic
D. Phase transitions
E. Raman spectroscopy
D. Structural and magnetic orders

ABSTRACT

Raman scattering spectra of $Ho_{1-x}Nd_xFe_3(BO_3)_4$ ($x=0$, $x=0.22$) crystals have been studied within 10–400 K temperature range. Structural phase transition was found under cooling at 366 K and 203 K respectively. Considerable modification in Raman spectra of the mixed crystal was found to be induced by magnetic ordering below Neel temperature. Results are interpreted using empirical simulation of crystal lattice dynamics and Raman intensities.



## 1. Introduction

In recent years crystals of rare-earth ferroborates (*Re* $Fe_3(BO_3)_4$, *Re* – rare-earth atom) received much attention. Owing to their high physical characteristics and chemical stability borates with huntite structure have long been used as elements of optical and optoelectronic devices, specifically, to sum and multiply laser radiation frequencies. Besides, they exhibit fairly unusual structural phase transition between nonpolar trigonal phases (from high-temperature $R32$ ($Z=1$) into the low-temperature $P3_221$ ($Z=3$)), while two magnetic ions of different types (3*d* and 4*f*) give rise to magnetic order at low temperatures [1]. Coexistence of structural and magnetic orders offers the potential of controlling their physical characteristics.

Interaction of structural and magnetic orders should, probably, have some effect on crystal lattice dynamics and observed in its vibrational spectrum. This work studies Raman spectra in the range of structural and magnetic phase transitions in $HoFe_3(BO_3)_4$ crystal and in $(Ho–Nd)Fe_3(BO_3)_4$ solid solution.

Fig. 1 [2] shows the structure of high symmetry phase of these crystals. It is formed by three helicoidal chains of $FeO_6$ octahedra with common edges linked by flat $BO_3$ triangles of two types with rare-earth ions in the cavities between them. These chains are the same in the high symmetry phase while in the low temperature phase $FeO_6$ octahedra are distorted slightly forming two different types of the chains (2+1). Structural phase transition in holmium ferroborate (unlike its relative crystals [3]) has never been studied by Raman spectroscopy, and is not observed in neodymium ferroborate; meanwhile the radii of these rare earth ions are quite different and such a replacement could be expected to lead to more marked effects.

## 2. Samples and Methods

Single crystal samples were grown from $Bi_2Mo_3O_{12}$-based flux melt [4,5]; that reduces replacement of rare-earth ions by bismuth to minimum. XFA analysis showed that bismuth content did not exceed 2% in the structure of synthesized samples. Solid solution was synthesized with a charge containing 25 at% of neodymium; analysis showed that produced single crystals correspond to $Ho_{0.78}Nd_{0.22}Fe_3(BO_3)_4$. Measurements were carried out on oriented single crystals sizing $1\times2\times1\ mm^3$, without defects or inclusions visible under microscope.

Raman spectra were studied with Horiba Jobin Yvon T64000 spectrometer in back scattering geometry in dispersion subtraction mode with entrance slit spectral resolution $2\ cm^{-1}$ (the resolution was attained by use of 1800 $mm^{-1}$ diffraction gratings and 100 μm slits). To study the soft mode near the phase transition the resolution was improved to $1.2\ cm^{-1}$.

The scattering spectrum was excited with $Ar^+$ laser (wavelength $\lambda=514$ nm) with 10 mW power on the sample which is equal to laser radiation density $30\ W/cm^2$. The power was chosen to minimize sample heating with acceptable signal/noise ratio in the spectra.

* Corresponding author. Tel.: +7 391 249 4510; fax: +7 391 243 8923.
*E-mail addresses:* shusy@iph.krasn.ru (A.S. Krylov), ssn@iph.krasn.ru (S.N. Sofronova), vtyurin@iph.krasn.ru (A.N. Vtyurin).

0038-1098/$ - see front matter © 2013 Elsevier Ltd. All rights reserved.
http://dx.doi.org/10.1016/j.ssc.2013.09.011

However, we still found phase transition temperature vs. exciting radiation power to shift linearly: $\Delta T = -(0.8 \pm 0.1)$ K/mW $\times P$ mW. Therefore, all temperature measurements were extrapolated to zero excitation power.

Temperature measurements were carried out with closed cycle ARS CS204-X1.SS helium cryostat in the temperature range 10–400 K. The temperature was monitored by LakeShore DT-6SD1.4L silicon diode; temperature stabilization accuracy was better than 0.1 K. Sample was placed into an indium pad open at one side and fixed to the cold finger of the cryostat. During experiments the cryostat was vacuumed to $10^{-6}$ mbar.

Quantitative analysis was carried out with Lorentz function:

$$I(\omega) = \frac{2}{\pi}\frac{A\Gamma}{4(\omega-\omega_0)^2+\Gamma^2} \quad (1)$$

where $A$, $\omega_0$, $\omega$, $\Gamma$ are the amplitude, position of the line center, wave number and full width at half maximum (FWHM), respectively.

## 3. Results and discussion

The room-temperature spectra of $HoFe_3(BO_3)_4$ for all studied experimental configurations are presented in Fig. 2. General view of the spectrum in the high-temperature phase for both crystals under study is shown in Fig. 3; it was analyzed in detail in [3]. We should note that the lines above 500 $cm^{-1}$ correspond to internal modes of $BO_3$ groups [3,6], and in all studied crystals of this family this part of the spectra virtually coincides. Compared to the spectrum of the free group [6] these lines are markedly split and shifted to the higher frequency range, indicating considerable effect of crystalline environment on them.

As the temperature decreases both crystals exhibit structural phase transition manifesting in several new lines emerging with lattice symmetry change. In $HoFe_3(BO_3)_4$ transition is observed at 366 K, which is somewhat lower than $T_c$=420 K, observed by authors of [1] and is probably related to different synthesis methods. In $Ho_{0.78}Nd_{0.22}Fe_3(BO_3)_4$ transition is shifted to 200 K. In analogy with crystals of other rare-earth ferroborates below the structural transition the soft phonon mode recovers (Fig. 4); however, the solid solution as opposed to the pure crystal does not exhibit hysteresis phenomena (or the hysteresis value is not more than 0.1 K), and condensation of the soft mode is attended by considerable damping anomaly – the latter might be due to numerous structural defects.

Below Neel temperature ($T_N$=38 K) both crystals are also observed to recover the soft modes (Fig. 4), earlier [3] this was explained by magnon scattering. Close temperatures of magnetic transitions and the recovery patterns of magnon soft modes in pure and mixed crystals indicate that their magnetic ordering is not related to the rare-earth subsystem and is determined by exchange interactions in Fe–O–Fe chains. In contrast to pure $HoFe_3(BO_3)_4$ crystal the mixed crystal below Neel temperature is also having marker rearrangement in the high-frequency spectrum. Most evident is the bending internal modes of $BO_3$ groups

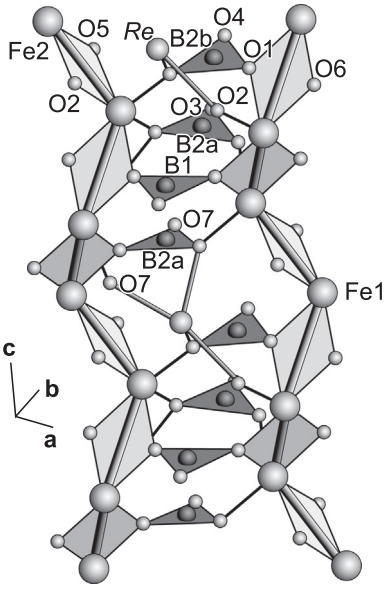


**Fig. 1.** Structure of high-symmetry phase of (Ho–Nd)$Fe_3(BO_3)_4$ crystals.

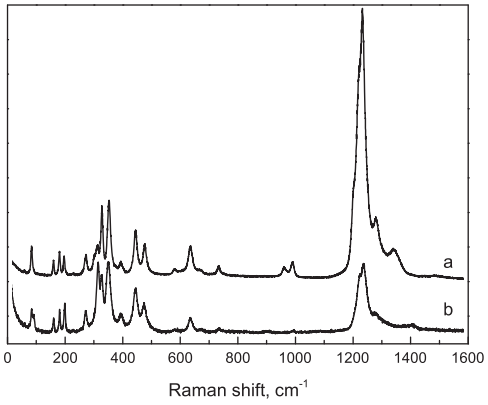


**Fig. 3.** General view of single crystal $b(ac)b$ polarized spectra at $R32$ phase: (a) Raman spectrum of $Ho_{0.78}Nd_{0.22}Fe_3(BO_3)_4$, $T$=296 K; (b) $HoFe_3(BO_3)_4$, $T$=380 K.

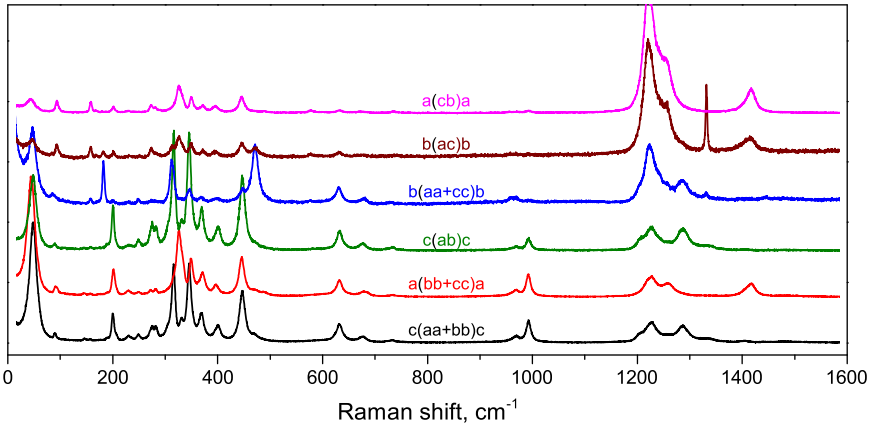


**Fig. 2.** (Color online) Polarized Raman spectra in the $P3_221$ phase of $HoFe_3(BO_3)_4$ at $T$=296 K.

about 600–650 $cm^{-1}$. Here emerge new lines whose intensity rapidly increases with decrease of temperature and becomes higher than that of neighboring lines (Fig. 5). Linear extrapolation of intensity vs. temperature to zero of the most intensive among these lines is in good agreement with Neel temperature – this undoubtedly is indicative of the determining role of magnetic ordering in the mechanism of their emergence.

Two-magnon scattering in the crystals of this family is observed in the range of 60–100 $cm^{-1}$ and there is no reason to assume that partial substitution of the rare-earth ion can considerably increase this frequency, because it is determined by exchange interactions in Fe–O–Fe chains, and the rare-earth subsystems do not markedly affect it. The most probable cause of this peak is the magnetoelastic interactions. It was assumed that below $T_N$ magnetoelastic interaction reduces the symmetry of crystal structure, and this can activate additional lines in the Raman spectrum [7]. However, the spectra of several pure *Re* $Fe_3(BO_3)_4$ (*Re*=Y, Nd, Pr) crystals [3] did not exhibit this effect, as the distortions of the structure caused by the weak magnetoelastic interaction seem to be too small to be recorded by Raman spectroscopy. In our case these structural changes are somewhat bigger than in the pure crystals because the solid solution was formed by rare-earth elements with essentially different ion radii (0.983 Å – Nd, 0.90 Å – Ho). Relatively small number of Nd increases the lattice parameters sufficiently for the O and B ions in Ho environment to have more freedom. The magnetoelastic interactions largely affect the shifts of oxygen ions immediately bonded with iron ions: O1, O2, O5 O6 [2] (see denotations in Fig. 1), and belonging to $BO_3$ groups. Lattice dynamics and Raman intensities of $HoFe_3(BO_3)_4$ crystal were empirically simulated [8] with lattice parameters of pure crystal structure and solid solutions; results of this simulation are given in Table 1.

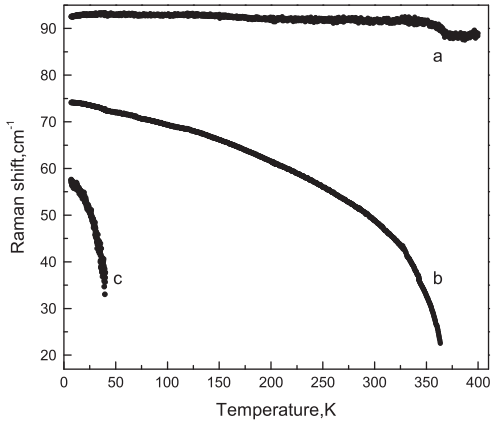


**Fig. 4.** Soft phonon mode recovery below structural transition in $HoFe_3(BO_3)_4$ crystal. (a) Hard mode; (b) structural soft mode; (c) magnon soft mode.

Within our model – rigid ion model – a crystal is considered to consist of isolated spherical ions with ionic charges $Z_i$, and the potential function is presented as a sum of non-Coulomb and electrostatic contributions:

$$U^{RIM} = U + \frac{1}{2}\sum_{i,j}\frac{Z_i Z_j}{r_{ij}}$$

Within this model only pair-wise interactions are considered. They are described by any analytical function $\phi(|R_{i,j}|)$ of interatomic distance $r_{ij}=x_i-x_j$. The corresponding potential function is expressed as $U=\sum_{i<j}\phi(r_{ij})$. The corresponding contributions to all the quantities can be easily expressed through two parameters and $\phi''=A$ and $B=\phi'/r$ (so-called longitudinal and transversal force constants).

The second energy derivative is

$$V_{ij} = U_{ij} - Z_i C_{ij} Z_j$$

where

$$C_{ij}^{\alpha\beta} = \frac{Z_i Z_j}{r_{ij}^3}\left(3\frac{r_{ij}^{\alpha} r_{ij}^{\beta}}{r_{ij}^2} - \delta_{\alpha\beta}\right),$$

$$U_{ij}^{\alpha\beta} = (A-B)\frac{r_{ij}^{\alpha} r_{ij}^{\beta}}{r_{ij}^2} + \delta_{\alpha\beta} B.$$

The electrostatic contribution was calculated by the Ewald method [9]. $U_{ij}$ was calculated by frame Born–Karman model (BKM) [10]. Two parameters of BKM are different for different pairs of ions (Table 2).

Lattice vibration calculation consists in evaluation and diagonalization of the dynamic matrix

$$D_{ij}^{\alpha\beta} = \frac{1}{\sqrt{m_i m_j}} V_{ij}^{\alpha\beta} \rightarrow \sum_j D_{ij} h_{jn} = \lambda_n h_{jn}$$

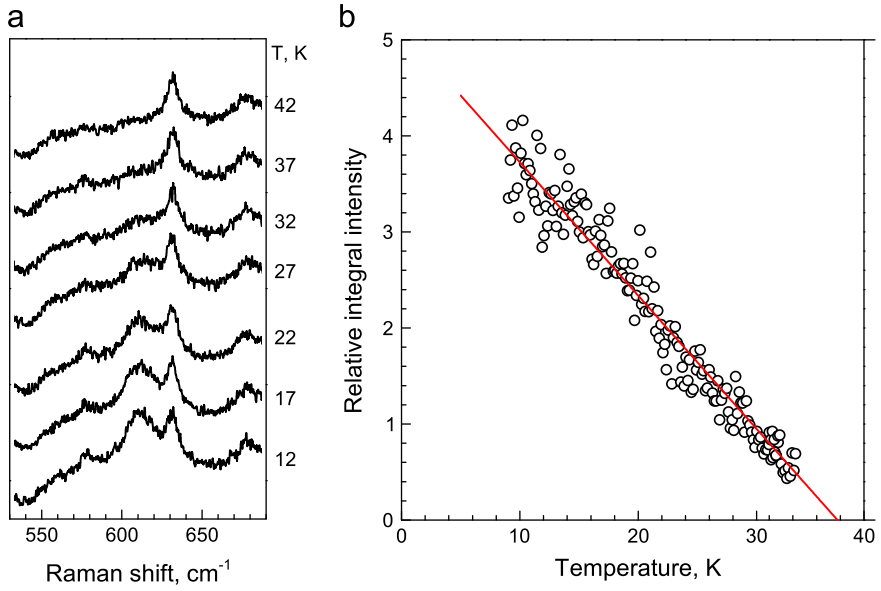


**Fig. 5.** (Color online) Intensity of lines vs. temperature in $Ho_{0.78}Nd_{0.22}Fe_3(BO_3)_4$. (a) Spectrum transformation; (b) relative intensity of $I_{611}/I_{631}$ lines with temperature.

**Table 1**
Frequencies $\omega$ ($cm^{-1}$) and relative intensities $I$ of Raman lines in the range 490–560 $cm^{-1}$, corresponding to internal vibrations of $BO_3$ groups calculated for the structure of pure $HoFe_3(BO_3)_4$ crystal and with oxygen ions shifted towards positions in the solid solution structure.

| Mode | Vibrating ions[a] | Displaced ions | | | | | | | | | | | |
|---|---|---|---|---|---|---|---|---|---|---|---|---|---|
| | | O2 | | | | O2, O5 | | O2, O5, O1 | | O1, O6 | | O2, O5, O1, O6 | |
| | | $\omega$ | $I$ | $\omega$ | $I$ | $\omega$ | $I$ | $\omega$ | $I$ | $\omega$ | $I$ | $\omega$ | $I$ |
| $A_1$ | O3,O4,O7 | 496.0 | 1.7 | 495.6 | 1.6 | 496.4 | 1.7 | 496.6 | 1.7 | 499.3 | 2.0 | 499.1 | 2.1 |
| $A_1$ | O5 | 541.1 | 1.3 | 540.7 | 1.6 | 545.5 | 1.7 | 545.5 | 1.7 | 543.2 | 0.7 | 541.6 | 0.6 |
| $A_1$ | O2,O7 | 555.9 | 2.3 | 554.7 | 2.2 | 557.0 | 2.1 | 557.0 | 2.1 | 561.7 | 1.5 | 562.3 | 1.5 |
| $E$ | O5 | 520.9 | 46.9 | 521.2 | 42.4 | 521.5 | 36.2 | 521.4 | 35.0 | 522.5 | 19.1 | 521.4 | 15.9 |
| $E$ | O4, O6, O7 | 524.9 | 13.5 | 522.5 | 19.2 | 526.3 | 12.0 | 527.5 | 12.7 | 527.3 | 19.2 | 526.3 | 25.8 |
| $E$ | O1 | 535.2 | 4.1 | 535.4 | 4.3 | 536.7 | 1.8 | 536.8 | 1.7 | 531.1 | 17.7 | 529.6 | 18.8 |
| $E$ | O1, O2 | 541.7 | 10.4 | 540.3 | 14.9 | 542.4 | 10.6 | 543.2 | 13.0 | 547.0 | 3.2 | 547.9 | 2.1 |
| $E$ | O2 | 551.3 | 11.9 | 550.6 | 12.8 | 552.3 | 12.8 | 553.1 | 10.5 | 557.2 | 10.5 | 558.1 | 9.9 |

[a] Given are the atoms with maximum contribution into eigenvector.

**Table 2**
Parameters of BKM for different pairs of ions.

| Ion | Ion | $A$ ($10^{-18}$j/Å) | $B$ ($10^{-18}$j/Å) |
|---|---|---|---|
| Ho | B | 340.17 | 0.40 |
| Ho | Fe | 250.17 | 0.383 |
| Ho | O | 350.17 | 0.40 |
| B | Fe | 350.17 | 0.40 |
| B | O | 288.17 | 0.27 |
| Fe | Fe | 250.17 | 0.383 |
| Fe | O | 380.17 | 0.40 |
| O | O | 275.17 | 0.39 |
| B | B | 250.17 | 0.34 |

where $\lambda_n$ – eigenvalues ($\omega_n = \sqrt{\lambda_n}$ the phonon frequencies) and $h_{jn}$ – eigenvectors.

Raman scattering intensity is

$$\zeta_n = \sum \varepsilon_i^{\infty} e_{in}$$

where mass-weighted eigenvectors:

$$e_{in} = \frac{1}{\sqrt{m_i}} h_{in}$$

atomic derivatives of the dielectric constant:

$$\varepsilon_i^{\infty} = \frac{d\varepsilon^{\infty}}{dx_i}$$

Table 1 presents vibration frequencies in the range 490–560 $cm^{-1}$, corresponding mostly to oxygen ions in $BO_3$ groups (the second column presents ions with the greatest shift during these vibrations). Then lattice dynamics of the same crystal was simulated – now with solid solution parameters and respective shift of ions O1, O2, O5 and O6. From the table it is apparent that the shift of oxygens to positions corresponding to the solid solution changes (several times) intensity of the Raman lines, while their frequencies remain practically invariable.

We assume that below Neel temperature in solid solution $Ho_{1-x}Nd_xFe_3(BO_3)_4$ due to increasing cell parameters the magnetoelastic interactions shift the oxygen ions more than in pure $HoFe_3(BO_3)_4$; this results in new additional lines in the Raman spectra and rapid growth of their intensity with magnetic ordering.

So, the authors were the first to observe considerable modification of Raman spectrum on lattice vibrations during magnetic ordering in $Ho_{1-x}Nd_xFe_3(BO_3)_4$ solid solution based on rare-earth ferroborate crystals.

## Acknowledgments

Authors are thankful to L.N. Bezmaternykh for useful discussion, A.V. Shabanov for his help in the analysis of sample chemistry. The work has been done with financial support of SS-4828.2012.2 grant, RFBR Foundation (Projects #11-02-98002, #12-02-00056), Federal Special Program "Scientific and scientific-pedagogical staff of innovative Russia" (# 8379).

## References

[1] Y. Hinatsu, Y. Doi, K. Ito, M. Wakeshima, A. Alemi, Journal of Solid State Chemistry 172 (2003) 438.
[2] C. Ritter, A. Vorotynov, A. Pankrats, G. Petrakovskii, V. Temerov, I. Gudim, R. Szymczak, Journal of Physics: Condensed Matter 20 (2008) 365209.
[3] D. Fausti, A. Nugroho, P.H.M. Loosdrecht, Physical Review B 74 (2006) 024403.
[4] L.N. Bezmaternykh, V.L. Temerov, I.A. Gudim, N.A. Stolbovaya, Crystallography Reports 50 (Suppl. 1) (2005) S97.
[5] L.N. Bezmaternykh, S.A. Kharlamova, V.L. Temerov, Crystallography Reports 49 (2004) 855.
[6] K. Nakamoto, Infrared and Raman Spectra of Inorganic and Coordination Compounds, Part A, 6th edn, John Wiley and Sons, New York (2009) 130–131.
[7] A.K. Zvezdin, S.S. Krotov, A.M. Kadomtseva, G.P. Vorobev, Y.F. Popov, A.P. Pyatakov, L.N. Bezmaternykh, E.A. Popova, JETP Letters 81 (2005) 272.
[8] M.B. Smirnov, V. Yu. Kazimirov, LADY: Software for Lattice Dynamics Simulations, Joint Institute for Nuclear Research Communications, Dubna, 2001.
[9] P. Ewald, Annalen der Physik 369 (1921) 253–287.
[10] Herman, Journal of Physics and Chemistry of Solids 8 (1959) 405.